Received: 7 December 2022 | Revised: 24 April 2023 | Accepted: 2 June 2023

DOI: 10.1111/jace.19289

Journal of the American Ceramic Society

RESEARCH ARTICLE

One-step fabrication of Li_2TiO_3 ceramic pebbles using pulsed YAG laser

Keisuke Mukai

Institute of Advanced Energy, Kyoto University, Uji, Kyoto, Japan

Correspondence
Keisuke Mukai, Institute of Advanced Energy, Kyoto University, Gokasho, Uji 611-0011, Kyoto, Japan.
Email: k-mukai@iae.kyoto-u.ac.jp

Funding information
Kansai Research Foundation for Technology Promotion; Grant-in-Aid for Scientific Research B from the Japan Society for the Promotion of Science (JSPS), Grant/Award Number: 23H01156

Abstract

A large amount of Li-containing ceramic breeder pebbles is packed in the solid breeding blanket of a nuclear fusion reactor. Several pebble fabrication technologies have been proposed in previous studies, including wet process, emulsion method, extrusion spheronization, additive manufacturing, and melt process. However, a simple, energy-effective, and scalable fabrication technology remains to be developed for the automated mass production and reprocessing of used radioactive pebbles post-operation. Selective laser melting potentially enables the quick and automated fabrication of breeder pebbles. Herein, we employ a high-power density pulse laser to produce ceramic breeder pebbles. A pulsed YAG laser was irradiated over a lithium metatitanate (Li_2TiO_3) powder bed in air, and the corresponding temperature was monitored using fiber-type infrared pyrometers. Spherical Li_2TiO_3 pebbles were successfully fabricated in a single step with an average diameter of 0.78 ± 0.13 μm and the sintering density of 87.4% ± 5.6% (input power: 7.9 J/pulse). The irradiated Li_2TiO_3 powder melted and turned spherical under surface tension and rapidly solidified, resulting in uniaxial fine grains and a decrease in the degree of long-range cation ordering.

KEYWORDS

Li-containing ceramics, Nd: YAG laser, nuclear fusion, pebble fabrication, selective laser melting

1 | INTRODUCTION

Nuclear fusion is a low-carbon and sustainable energy source by fusing hydrogen isotopes of deuterium and tritium. Tritium is a rare and radioactive isotope, so it is produced by Li-containing compounds in breeding blankets surrounding the fusion plasma.[1] The solid breeding blanket concept has been developed for a demonstration (DEMO) fusion reactor using Li-containing ceramic breeder pebbles with a cooling system using pressurized water or helium to validate fuel self-sufficiency.[2–5] A significant amount of Li-containing pebbles, that is, one or two hundred tons,[6,7] will be packed in a DEMO fusion reactor. The most promising materials of ceramic breeder are Li_2TiO_3, Li_4SiO_4, and these mixture, in which ^6Li is enriched to 60–90 at.% to ensure the amount of tritium bred in the blanket is greater than that consumed in the plasma. The pebbles used after an operational period of 2–5 years are expected to be reprocessed after a cooling period, refabricated, and reused, because (1) ^6Li-enriched

compounds are highly expensive and (2) the average burn up of ^{6}Li in the breeding blanket is only ~1% per full power year in a DEMO reactor.[8] Hence, a simple, inexpensive, and scalable fabrication method is desirable for the mass fabrication and re-fabrication using the activated pebbles.

Dense and spherical ceramic breeder pebbles are required for breeding and releasing fuel tritium efficiently as well as for reducing thermal stress in the pebble bed blanket. Several techniques have been proposed for the fabrication of ceramic breeder pebbles. The wet process[9–12] is a well-established method which can produce spherical green pebbles by dropping a liquid mixture of Li_2TiO_3 and polyvinyl-alcohol through a nozzle. In the emulsion method,[13–15] green pebbles with a narrow size distribution are produced by cutting the Li_2TiO_3 slurry flow with oil flow in a T-shaped flow path. The extrusion spheronization method[16–18] forms green pebbles from mixture of raw powder and polyvinyl-alcohol binder using a Spherodizer. Additive manufacturing[19,20] is an emerging technique, which employs ultraviolet light or a CO_2 laser to form green pebbles. However, these methods mentioned above involve multiple processes composed of spherization of green pebbles, drying for debinding, calcination (optional), and sintering at >1000°C using time and energy-consuming electric furnaces. Melt process[21–23] is a one-step fabrication method by heating breeder materials above the melting point in a noble metal crucible. Then, the melt is dropped and solidified in a cooling tower by spraying liquid nitrogen. Although this method enables a reprocessing after service,[24] the fabrication via the harsh process has technical challenges in controlling the pebble size distribution and improving the crush load.

Additionally, breeder pebbles are required to have a small grain size, preferably <5 μm.[6,14] This is because the diffusion of tritium ions within the crystal grain is one of the rate-determining steps in the whole tritium release processes.[25–27] Based on the classical solidification theory of Kurz and Fischer,[28] the microstructure and size of grains are influenced by the solidification rate R and local temperature gradient G. The cooling rate $\dot{T}$ ($\dot{T} = G/R$) governs the scale of the microstructure, thus a fabrication method with a rapid cooling may lead to a decrease in the grain size. Herein, we propose a new fabrication method using a high-power neodymium-doped yttrium aluminum garnet (Nd: YAG) laser, in which Li_2TiO_3 breeder pebbles are directly fabricated from the powder bed by a single step. The effects of input power on the size distribution, the microstructure, and crystal structure of the fabricated pebbles are investigated. Based on the results, pebble formation mechanism and energy efficiency are discussed.

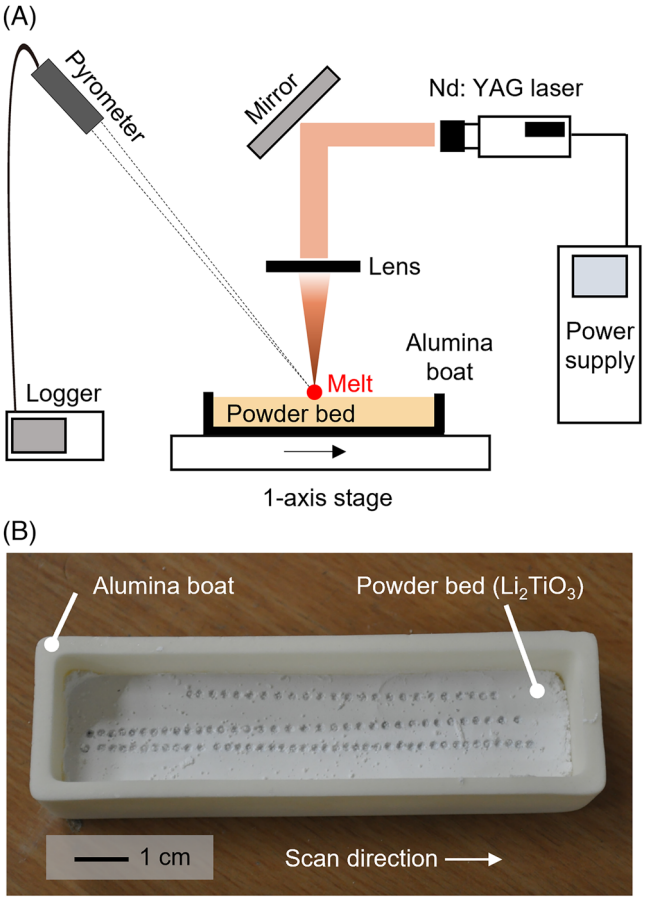

FIGURE 1 Schematic diagram of the experimental set up (A) and sample powder bed after irradiations (B). Nd: YAG laser was irradiated onto a Li_2TiO_3 powder bed in an alumina boat where temperature of the laser spot was monitored using the single- or two-color pyrometers and recorded by a data logger.

2 | METHODS

Ceramic breeder pebbles were fabricated by irradiating an Nd: YAG laser (wavelength: 1064 nm) on to a Li_2TiO_3 powder bed as shown in Figure 1. Super Laser MAX-S30P (THM Co., Ltd.) was used as a high-power pulse laser source. The laser spot size was 1.2 mmϕ. The maximum peak output and pulse repetition rate were 30 J/pulse and 30 pulse/s, respectively. The pulse width was set 2.5 ms in this work. Li_2TiO_3 powder (>99%) was procured from Kojundo Chemical Laboratory Co., Ltd. The grain size distribution of the initial powder is shown in Figure S1. The average size was estimated to be 0.53 μm with standard deviation 0.16 μm. The powder was filled in an alumina boat and pressed with a plate to make a flat surface. The density of the powder bed was 1.39 g/cm^3, approximately 40% of the theoretical density of Li_2TiO_3. The boat was placed on a one-axis stage. The temperature of the laser spot was monitored using two infrared radiation pyrometers. One was a fiber-optic single-color pyrometer (Japan

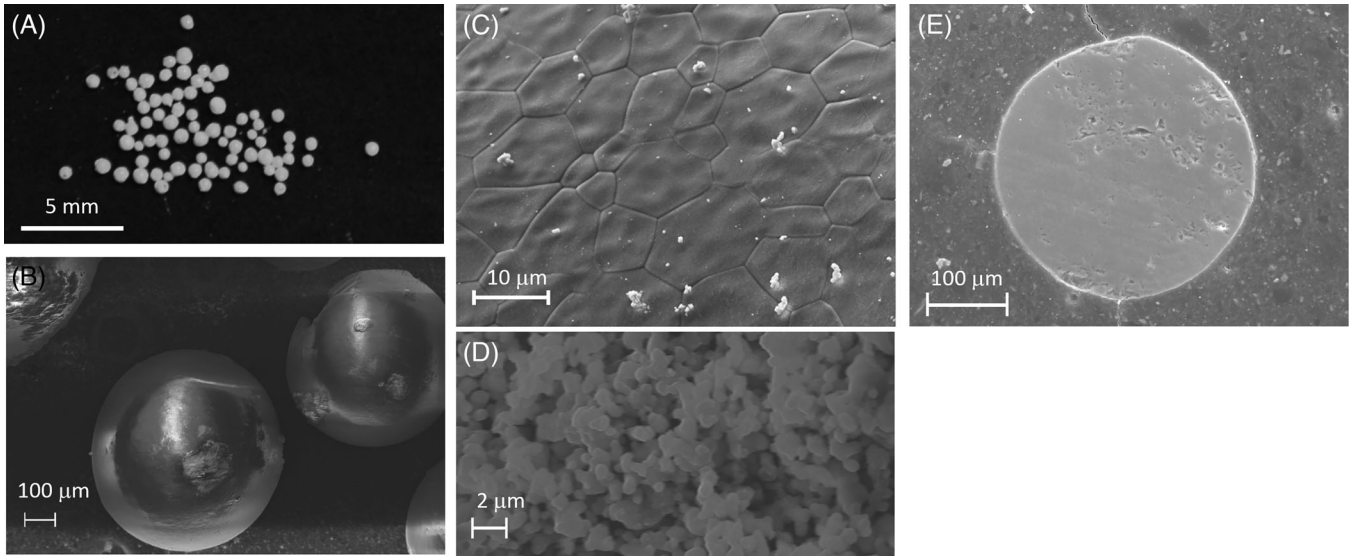

FIGURE 2 Photo (A), scanning electron microscope (SEM) images of the surface (B and C), inside grains (D), and the cross-section (E) of the pebbles fabricated with the laser power of 7.9 ± 0.1 J/pulse.

Sensor Co.) with an InGaAs image sensor, covering 180–2000°C with a target size of 1.8 mmϕ. The output voltage range was from 0 to 1 V and had a linear relationship with the measured temperature. The emissivity for the single-color pyrometer was set to be 1.0. The other was a fiber-optic two-color pyrometer with Si and InGaAs image sensors, covering 700–2000°C with a target size of 5 mmϕ. The single- and two-color pyrometers were used for measuring the heating/cooling rate and maximum temperature, respectively. The outputs from the single-color and two-color pyrometers were recorded using a data logger with sampling rates of 100 and 10 ms, respectively.

The Li_2TiO_3 powder bed was irradiated in air with the pulse powers of 7.1, 8.2, 9.3, and 10.3 J. After a pulse irradiation, the powder bed in the alumina boat was moved ~2.5 mm by using the one-axis stage and then irradiated again (Figure 1B). This procedure was repeated for 100 times in each input-power condition. After the fabrication process, the pebbles were collected by using a sieve with a mesh size of 300 μm. The densities of the pebbles were measured by helium pycnometry by Micromeritics (AccuPyc II 1340). Uniaxial crush load tests were carried out for single pebble with a crosshead speed of 0.01 mm/min. The surface of the pebbles was observed by using scanning electron microscope (SEM). For the cross-section observations, the pebbles were embedded in an electrically conductive resin and then polished with sandpaper. Powder X-ray diffraction (XRD) was carried out with Rigaku TTR-III using Co–K_α radiation. The XRD patterns from the powder prepared by crushing the pebbles in an agate mortar as well as the original powder were collected in the 2θ range of 20–100° at a step of 0.02°. Theoretical XRD patterns of monoclinic and cubic Li_2TiO_3 were simulated by using the crystal structure data by Kataoka et al.[29] and Laumann et al.,[30] respectively. VESTA software was used for the simulations of XRD pattern and visualization of the crystal structures.[31] The initial powder and fabricated pebbles were dissolved with HCl and H_2SO_4. The solution was mixed with dilute HNO_3. The concentrations of Li and Ti were quantified using inductively coupled plasma optical emission spectroscopy (ICP-OES).

3 | RESULTS

Figure 2 shows the pebbles fabricated by YAG laser irradiation at a laser power of 7.9 J/pulse. The pebbles fabricated by the one-step process had spherical shapes with a diameter size distribution (Figure 2A). The surfaces of the fabricated pebbles were observed via SEM to be smooth (Figure 2B), indicating heating and melting of the irradiated part (melting temperature of Li_2TiO_3: 1533°C[32]) followed by the solidification during cooling. The SEM images in Figure 2C,D show that the grain sizes of the surface and inside of the pebble were 9.4 and ~1 μm, respectively. The surface had a growth of crystal grains, whereas the inside grain size was almost the same as that of the original Li_2TiO_3 powder before irradiation. The SEM image of the cross-section in Figure 2E represents the pebble to be spherical with a dense microstructure and micrometer-sized closed pores.

Figure 3 shows the temporal temperature change in the laser spot measured by the two pyrometers. The output voltage from the single-color pyrometer exhibits a linear

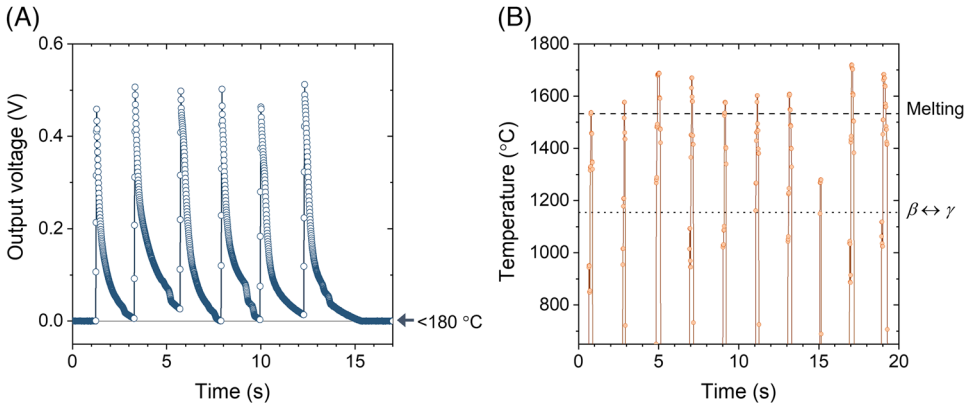

FIGURE 3 Output voltage from the single-color pyrometer (A) and temperature measured by the two-color pyrometer (B) during YAG laser irradiations with the laser power of 7.9 ± 0.1 J/pulse, in which dotted and broken lines denote the temperatures of β–γ transformation and melting point of Li_2TiO_3.

relationship with the temperature, such that 0 and 1 V correspond to 180 and 2000°C, respectively. Although the emissivity ε of Li_2TiO_3 at high temperatures is not found from literatures, an emissivity of 0.8–0.95 was assumed in this study. In the previous measurement for $Li_4Ti_5O_{12}$, an emissivity of 0.8–0.9 was assumed for the temperature range of 703–964°C.[33] The output voltage measured by the single-color pyrometer with $\varepsilon = 1.0$ with the power condition of 7.9 J/pulse is shown in Figure 3A. During the laser irradiations, the voltage reached to the maxima in approximately 0.5 s and then decreased to 0 V (<180°C) in ~2 s, indicating a rapid heating/cooling of the irradiated spot. The maximum voltage was ~0.5 V, corresponding to 1090°C. However, this temperature was significantly below the melting temperature of Li_2TiO_3 (1533°C) and inconsistent with the SEM surface observation results. Hence, the maximum temperature was measured by the two-color pyrometer as shown in Figure 3B, wherein $\varepsilon = 0.8$. It is seen that the maximum temperature reached above the melting point in the most cases. At the irradiation at $t \sim 15$ s, the temperature did not reach the melting point despite being heated up to it. This is presumably because the melt flowed away from the measuring spot upon gas release. Using the two-color pyrometer, the maximum temperature was measured to be 1577–1720°C by assuming $\varepsilon = 0.8$. The temperature rapidly decreased from the maxima to 700°C (0 V output) in 0.2–0.3 s. Given a maximum temperature is 1600°C, it corresponds to a cooling rate of $\dot{T} = 3000$–4500°C/s. The temperatures monitored by the two-color pyrometer by setting $\varepsilon = 0.9$ and 1.0 were also measured (Figure S2). The temperature of the spot was above the melting point even with the emissivity values.

In Figure 4, the size distribution of the fabricated pebbles with the pulse powers of 6.9, 7.9, 9.0, and 9.8 J are shown. The deviation in the input energy was less than 0.1 J. In total, $n = 59$–74 pebbles were collected after sieving the powder bed, whereas laser was irradiated 100 times in each energy condition. This is because (1) some pebbles were jumped away from the powder bed upon gas release and (2) pebbles smaller than the mesh size (300 μm) were not collected by the sieve. The average pebble diameters were 856 ± 163 μm (6.9 J), 784 ± 125 μm (7.9 J), 714 ± 121 μm (9.0 J), and 694 ± 148 μm (9.8 J). Although the average diameters appeared to decrease with the power, the relationship between the power and size is unclear owing to the large deviations. The sintering densities were measured to be 82.3% ± 3.1% (6.9 J), 87.8% ± 5.6% (7.9 J), 90.6% ± 14.5% (9.0 J), and 80.0% ± 18.8% (9.8 J) of the theoretical density (3.43 g/cm^3). The large error in the pebbles with 9.0 and 9.8 J was owing to the substantially small weight of the samples, that is, approximately 10 mg.

Li/Ti ratios of the fabricated pebbles with the laser power of 7.3, 9.0, and 9.8 J were given to be 1.84 ± 0.01, 1.76 ± 0.01, and 17.5 ± 0.01, whereas that of the initial powder was 1.94 ± 0.03. The ratio decreased due to the evaporation of Li during the laser. The mean crush loads of the pebbles fabricated with 6.9 and 7.9 J input conditions were 7.7 ± 4.7 N ($n = 20$) and 5.6 ± 2.8 N ($n = 18$), respectively. These values were low compared with the Li_2TiO_3 pebbles fabricated by the other methods and similar to those of Li_4SiO_4–Li_2TiO_3 biphasic pebbles fabricated by melt process; the crush loads of Li_2TiO_3 pebbles by emulsion method,[34] Li_2TiO_3 pebbles by piezoelectric microdroplet jetting,[11] Li-rich Li_2TiO_3 pebbles by rolling method,[35] and Li_4SiO_4–Li_2TiO_3 pebbles by melt process[24] are 37.2, 25.7, 10–41, and 5–15 N. Crush load of the pebbles could be improved by an additional heat treatment and/or compositional modification, as reported in the previous studies.[22,36] Particularly, an addition of Li_2CO_3 to the initial powder as a sintering aid may contribute both to densification and increase of Li/Ti ratio.[37]

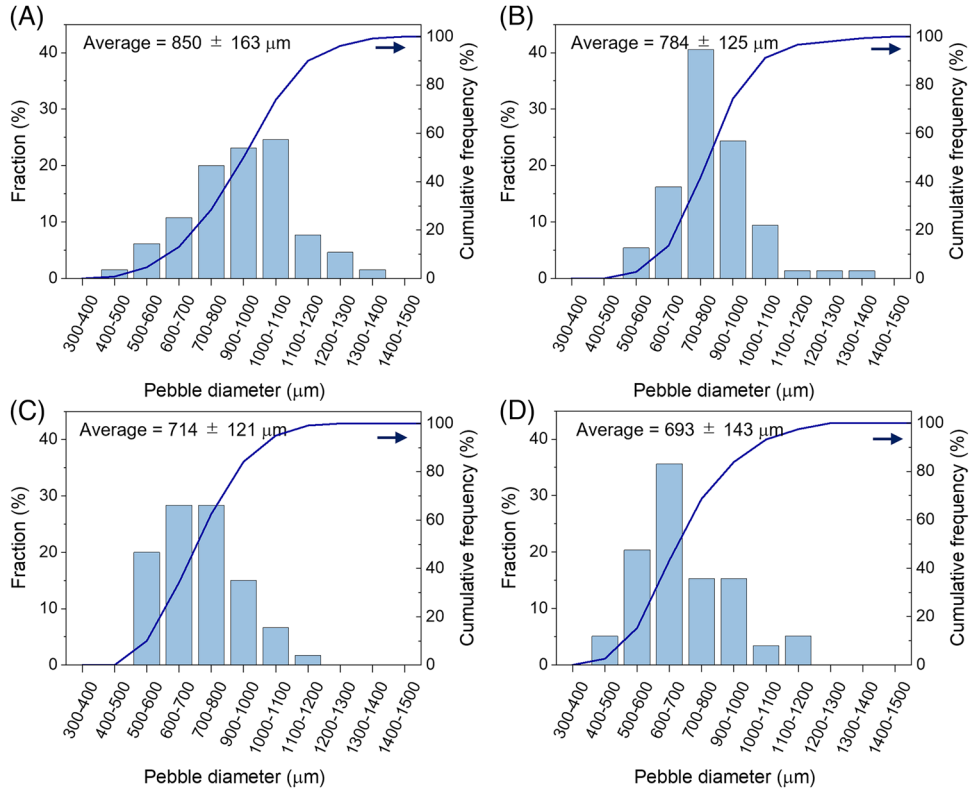

FIGURE 4 Size distributions of the pebbles fabricated with the laser powers of 6.9 J (A), 7.9 J (B), 9.0 J (C), and 9.8 J (D).

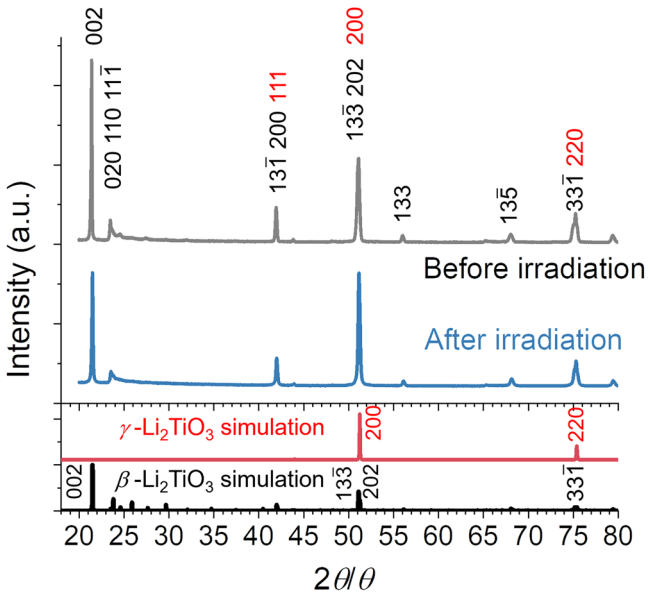

FIGURE 5 Comparison of the X-ray diffraction patterns of the Li_2TiO_3 powders before and after YAG laser irradiations with the simulated patterns of β-Li_2TiO_3 and γ-Li_2TiO_3.

Figure 5 compares the XRD patterns of the powder prepared by crushing the pebbles (laser power: 7.9 J) with the data of original powder and simulated patterns of β- and γ-Li_2TiO_3. As a result, no new peak was found from the irradiated sample. This indicates that the change in the composition caused by vaporization is insignificant. Additionally, the formation of impurity phase such as Li_2CO_3 was not found even with the fabrication in air. A change in the peak intensities was observed before and after irradiation; this point is discussed in the following section.

4 | DISCUSSION

The XRD data in Figure 5 shows the peak intensity from the (0 0 2) plane of β phase to become weaker in the irradiated sample. This peak is designated as peak A in this paper, which corresponds to the long-range ordering of the Li–Ti–O layers along the c axis (d spacing: ~4.8 Å) in β-Li_2TiO_3. In contrast, the diffraction intensity from the irradiated sample at 51.2° is stronger than that of peak A. This peak is designated as peak B in this paper, which is derived from the main peak of γ-Li_2TiO_3 from (2 0 0) plane as well as (1 3 3) and (2 0 2) planes in β-Li_2TiO_3. The intensity ratio of peak A and B, I_A/I_B, represents the degree of long-range cation ordering.[38,39] Although the I_A/I_B ratios were 2.4 and 0.0 in the simulated patterns from the perfect crystals of β- and γ-Li_2TiO_3, the ratios from the samples before and after irradiations were 2.0

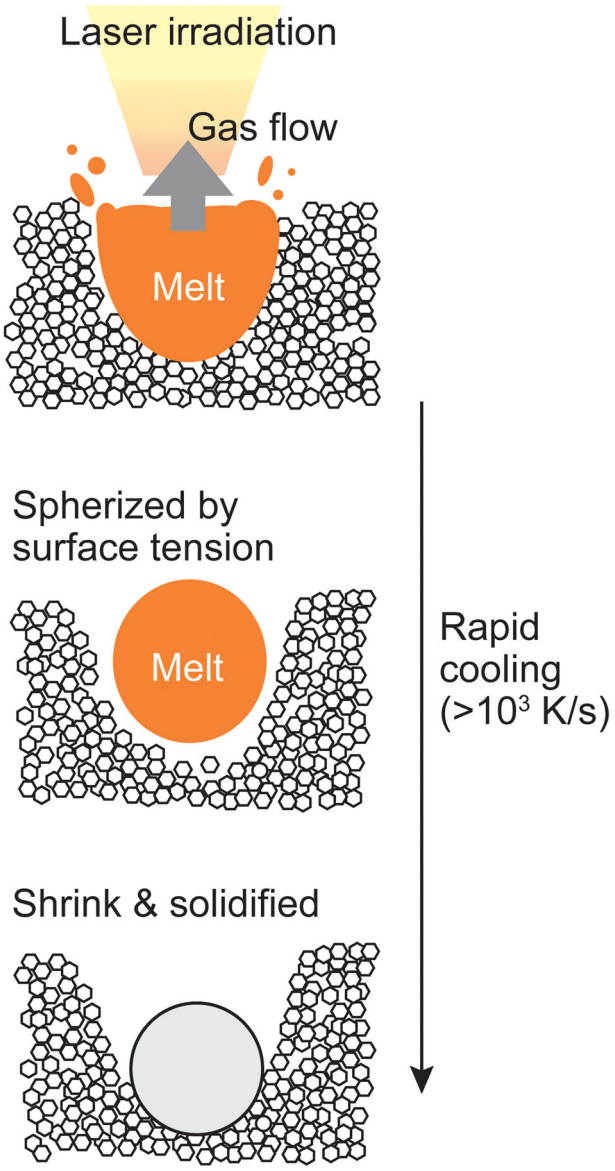

FIGURE 6 Schematic image of morphological changes upon a YAG laser irradiation.

and 1.0, respectively. This indicates that the degree of the cation ordering decreased after irradiation. This is ascribed to the quenching of the high-temperature γ phase by the rapid cooling of the melt. The cooling rate of this fabrication method was 3000–4500°C/s and significantly faster (i.e., by several orders of magnitude) than the one in a fabrication process using an electronic furnace. This could be a reason that a small grain size is observed in Figure 2D.

From the experimental results, the formation mechanisms of the spherical pebble and crystal structural change upon laser irradiation are drawn as Figure 6. The irradiated spot is rapidly heated up above the melting point in <0.5 s, while releasing gases such as water vapor and CO_2. The melt becomes spherical because of surface tension and then solidifies, with a significantly rapid cooling rate. Given that there is a temperature difference of 1500°C between the irradiation spot and a position 3 mm away from the spot center, the local temperature gradient G is estimated to be 500°C/mm. Using the values of G and $\dot{T}$, the solidification map predicts that fine and uniaxial grains are formed by this laser process. This prediction is consistent with the small grains without orientation observed by SEM (Figure 2C).

To investigate the energy efficiency of this fabrication method, the energy consumed E for each laser irradiation was estimated. It was assumed that, with the input laser energy of 7.9 J, a melt is heated from 25 to 1600°C and then a pebble with a diameter of 0.75 mm and density of 85% is fabricated. The energy consumption to fabricate the pebble (E) is given as follows:

$$E = m\left\{\int_{25}^{1155} c_{\mathrm{p},\beta}(\mathrm{T})\mathrm{d}T + \int_{1155}^{1533} c_{\mathrm{p},\gamma}(\mathrm{T})\mathrm{d}T + \int_{1533}^{1600} c_{\mathrm{p,m}}(\mathrm{T})\mathrm{d}T + \Delta H_{\mathrm{tr}}/M + \Delta H_{\mathrm{m}}/M\right\} \quad (1)$$

where m, M, $c_{\mathrm{p},\beta}$, $c_{\mathrm{p},\gamma}$, and $c_{\mathrm{p,m}}$ denote the mass of single-pebble, molecular weight, heat capacities of β, γ, and melt phases of Li_2TiO_3. ΔH_{tr} and ΔH_{m} are the enthalpies of the β–γ transformation and melting, respectively. These enthalpies were taken from the literatures as ΔH_{tr} = 9.2 kJ/mol[40] and ΔH_{m} = 110 kJ/mol.[41] The temperature dependencies of $c_{\mathrm{p},\beta}(T)$ and $c_{\mathrm{p},\gamma}$ (T) were given by Kleykamp et al.,[40] whereas $c_{\mathrm{p,m}}(T)$ was assumed to be equivalent to $c_{\mathrm{P},\gamma}(T)$ because the heat capacity of the liquid phase was not found in the literatures. To this end, the consumed energy was estimated to be 2.1 J per pebble, corresponding to 26% of the laser power.

The energy consumption is compared with that for sintering $BaTiO_3$, because the literature data of Li_2TiO_3 was not found. The heat capacity of $BaTiO_3$ is 102.4 J/mol/K at 27°C[42] and similar to that of Li_2TiO_3 (c_p = 108.6 J/mol/K at 25°C[40]). The energy consumption for fabricating Li_2TiO_3 by the laser process corresponds to 12.7 kJ/g, which is significantly lower than 2800 kJ/g for sintering $BaTiO_3$ at 1300°C by conventional method using electric furnace in a lab-scale condition.[43] However, this advantage is only valid on gram basis, because the conventional process could be more energy-efficient by scaling up, whereas that of the laser process should remain constant. Hence, the energy consumptions for 5 kg are compared. The laser process consumes 63.5 MJ for 5 kg of Li_2TiO_3 pebbles, which surpass the total energy consumption for $BaTiO_3$ by conventional sintering estimated by T. Ibn-Mohammed et al. to be 990 MJ.[44] This comparison shows that the laser

process still has advantage in energy consumption by one order of magnitude on kilogram basis.

5 | CONCLUSIONS

This study proposes a one-step fabrication method for Li_2TiO_3 pebbles using a pulsed Nd: YAG laser. After the irradiation onto the powder bed, the corresponding spot was rapidly heated up (in less than 0.5 s) above the melting point, while releasing gases from the melt. The melt turned spherical because of surface tension followed by a rapid solidification, which increased the degree of long-range cation disorder by the quenching. The average pebble diameters were 694–856 μm, and the sintering densities were 80%–91% of the theoretical density (i.e., 3.43 g/cm^3). The pebbles exhibited uniaxial and fine grains as large as 1 μm because of the extremely high-temperature gradient and rapid cooling rate. The advantage of this method is not only a simple process but also a high energy efficiency 12.7 kJ/g (~26% of the input laser power), which could be applied to an automated fabrication. The remaining challenge lies in the compositional change and the mechanical property of the fabricated pebbles, which may be improved by an additional heat treatment and/or by mixing with additives.

ACKNOWLEDGMENTS

This study was financially supported by Kansai Research Foundation for Technology Promotion and a Grant-in-Aid for Scientific Research B (23H01156) from the Japan Society for the Promotion Science (JSPS). Prof. S. Konishi and Prof. J. Yagi at Kyoto University, and Prof. T. Takayama at National Institute for Fusion Science are thanked for fruitful discussions. R. Ito and S. Aratani at Kyoto University are thanked for technical support for the ICP measurements.

CONFLICT OF INTEREST STATEMENT

The author declares no conflict of interest.

ORCID

Keisuke Mukai https://orcid.org/0000-0001-8067-8732

REFERENCES

1. Lee WE, Gilbert M, Murphy ST, Grimes RW. Opportunities for advanced ceramics and composites in the nuclear sector. J Am Ceram Soc. 2013;96:2005–30. https://doi.org/10.1111/jace.12406
2. Hernández FA, Pereslavtsev P, Zhou G, Kang Q, D'Amico S, Neuberger H, et al. Consolidated design of the HCPB breeding blanket for the pre-conceptual design phase of the EU DEMO and harmonization with the ITER HCPB TBM program. Fusion Eng Des. 2020;157:111614. https://doi.org/10.1016/j.fusengdes.2020.111614
3. Zhuang G, Li GQ, Li J, Wan YX, Liu Y, Wang XL, et al. Progress of the CFETR design. Nucl Fusion. 2019;59:112010. https://doi.org/10.1088/1741-4326/ab0e27
4. Yun S, Park SD, Lee DW, Lee CW, Jin HG, Shin CW, et al. Conceptual design and analysis of the HCCR breeder blanket for the K-DEMO. Fusion Eng Des. 2020;153:111513. https://doi.org/10.1016/j.fusengdes.2020.111513
5. Tobita K, Hiwatari R, Sakamoto Y, Someya Y, Asakura N, Utoh H, et al. Japan's efforts to develop the concept of JA DEMO during the past decade. Fusion Sci Technol. 2019;75:372–83. https://doi.org/10.1080/15361055.2019.1600931
6. Konishi S, Enoeda M, Nakamichi M, Hoshino T, Ying A, Sharafat S, et al. Functional materials for breeding blankets—status and developments. Nucl Fusion. 2017;57:092014. https://doi.org/10.1088/1741-4326/aa7e4e
7. Boccaccini LV, Arbeiter F, Arena P, Aubert J, Bühler L, Cristescu I, et al. Status of maturation of critical technologies and systems design: breeding blanket. Fusion Eng Des. 2022;179:113116. https://doi.org/10.1016/j.fusengdes.2022.113116
8. Mukai K, Pereslavtsev P, Fischer U, Knitter R. Activation calculations for multiple recycling of breeder ceramics by melt processing. Fusion Eng Des. 2015;100:565–70. https://doi.org/10.1016/j.fusengdes.2015.08.007
9. Tsuchiya K, Kawamura H, Fuchinoue K, Sawada H, Watarumi K. Fabrication development and preliminary characterization of Li_2TiO_3 pebbles by wet process. J Nucl Mater. 1998;258–263:1985–90. https://doi.org/10.1016/S0022-3115(98)00229-3
10. Tan G, Hu X, Wang S, Yang X, Li Y, Yang Z, et al. A process for fabrication of Li2TiO3 ceramic pebbles with high mechanical properties via non-hydrolytic sol-gel method. Ceram Int. 2020;46:27686–94. https://doi.org/10.1016/j.ceramint.2020.07.266
11. Cai J, Xu G, Lu H, Xu C, Hu Y, Cai C, et al. Preparation of tritium breeding Li_2TiO_3 ceramic pebbles via newly developed piezoelectric micro-droplet jetting. J Am Ceram Soc. 2022;105:3753–64. https://doi.org/10.1111/jace.18320
12. Yang M, Wang H, Chen R, Gong Y, Huang Z, Ran G, et al. Comparison of the microwave and conventional sintering of Li_2TiO_3 ceramic pebbles. Ceram Int. 2018;44:19672–7. https://doi.org/10.1016/j.ceramint.2018.07.219
13. Hoshino T, Nakamichi M. Development of fabrication technologies for advanced breeding functional materials for DEMO reactors. Fusion Eng Des. 2012;87:486–92. https://doi.org/10.1016/j.fusengdes.2012.01.005
14. Hoshino T, Edao Y, Kawamura Y, Ochiai K. Pebble fabrication and tritium release properties of an advanced tritium breeder. Fusion Eng Des. 2016;109–111:1114–8. https://doi.org/10.1016/j.fusengdes.2016.01.012
15. Kolb MHH, Mukai K, Knitter R, Hoshino T. Li_4SiO_4 based breeder ceramics with Li_2TiO_3, $LiAlO_2$ and $LiXLaYTiO_3$ additions, Part I: Fabrication. Fusion Eng Des. 2017;115:39–48. https://doi.org/10.1016/j.fusengdes.2016.12.033
16. Lulewicz JD, Roux N. Fabrication of Li_2TiO_3 pebbles by the extrusion–spheronisation–sintering process. J Nucl Mater. 2002;307–311:803–6. https://doi.org/10.1016/S0022-3115(02)00981-9
17. Sahu BS, Adhikari P, Gorinta J, Choudhary A, Mazumder R, Bhattacharyya S, et al. Fabrication and characterization of Li_2TiOb_3 pebbles by an extrusion and spherodization technique for the test blanket module in a fusion reactor. Fusion Sci Technol. 2014;65:338–45. https://doi.org/10.13182/FST13-671
18. Jaya Rao G, Mazumder R, Bhattacharyya S, Chaudhuri P. Fabrication and characterization of Li_4SiO_4-Li_2TiO_3

composite ceramic pebbles using extrusion and spherodization technique. J Eur Ceram Soc. 2018;38:5174–83. https://doi.org/10.1016/j.jeurceramsoc.2018.07.018
19. Zhou Q, Gao Y, Liu K, Xue L, Yan Y. Fabrication of Li2TiO3 pebbles by a selective laser sintering process. Fusion Eng Des. 2015;100:166–70. https://doi.org/10.1016/j.fusengdes.2015.05.061
20. Cai L, Hu X, Tan G, Li G, Zhang Y. Accurate and uniform fabrication of Li_2TiO_3 pebbles with high properties based on stereolithography technology. J Eur Ceram Soc. 2021;41:2114–23. https://doi.org/10.1016/j.jeurceramsoc.2020.10.050
21. Knitter R, Kolb MHH, Kaufmann U, Goraieb AA. Fabrication of modified lithium orthosilicate pebbles by addition of titania. J Nucl Mater. 2013;442:S433–6. https://doi.org/10.1016/j.jnucmat.2012.10.034
22. Zhai Y, Hu J, Duan Y, Wang K, Zhang W. Characterization of tritium breeding ceramic pebbles prepared by melt spraying. J Eur Ceram Soc. 2020;40:1602–12. https://doi.org/10.1016/j.jeurceramsoc.2019.12.021
23. Leys O, Leys JM, Knitter R. Current status and future perspectives of EU ceramic breeder development. Fusion Eng Des. 2021;164:112171. http://doi.org/10.1016/j.fusengdes.2020.112171
24. Leys O, Bergfeldt T, Kolb MHH, Knitter R, Goraieb AA. The reprocessing of advanced mixed lithium orthosilicate/metatitanate tritium breeder pebbles. Fusion Eng Des. 2016;107:70–4. https://doi.org/10.1016/j.fusengdes.2016.04.025
25. Tanifuji T, Yamaki D, Nasu S, Noda K. Tritium release behavior from neutron-irradiated Li_2TiO_3 single crystal. J Nucl Mater. 1998;258–263:543–8. https://doi.org/10.1016/S0022-3115(98)00103-2
26. Kobayashi M, Oya Y, Okuno K. Tritium trapping states induced by lithium-depletion in Li_2TiO_3. J Nucl Mater. 2017;487:84–90. https://doi.org/10.1016/j.jnucmat.2017.02.008
27. Katayama K, Someya Y, Tobita K, Fukada S, Hatano Y, Chikada T. Influence of hydrogen addition to a sweep gas on tritium behavior in a blanket module containing Li_2TiO_3 pebbles. Fusion Eng Des. 2016;113:221–6. https://doi.org/10.1016/j.fusengdes.2016.08.031
28. Kurz W, Fischer DJ. Fundamentals of solidification. 4th ed. Wollerau: Trans Tech Publications Ltd; 1998.
29. Kataoka K, Takahashi Y, Kijima N, Nagai H, Akimoto J, Idemoto Y, et al. Crystal growth and structure refinement of monoclinic Li_2TiO_3. Mater Res Bull. 2009;44:168–72. https://doi.org/10.1016/j.materresbull.2008.03.015
30. Laumann A, Fehr KT, Boysen H, Hoelzel M, Holzapfel M. Temperature-dependent structural transformations of hydrothermally synthesized cubic Li_2TiO_3 studied by in-situ neutron diffraction. Z Kristallogr. 2011;226:53–61. https://doi.org/10.1524/zkri.2011.1286
31. Momma K, Izumi F. VESTA 3 for three-dimensional visualization of crystal, volumetric and morphology data. J Appl Crystallogr. 2011;44:1272–6. https://doi.org/10.1107/S0021889811038970
32. Kleykamp H. Phase equilibria in the Li-Ti-O system and physical properties of Li_2TiO_3. Fusion Eng Des. 2002;61–62:361–6. https://doi.org/10.1016/S0920-3796(02)00120-5
33. Liu F, Bai B, Cheng L, Xu C. Rapid synthesis of $Li_4Ti_5O_{12}$ as lithium-ion battery anode by reactive flash sintering. J Am Ceram Soc. 2022;105:419–27. https://doi.org/10.1111/jace.18086
34. Hoshino T. Trial examination of direct pebble fabrication for advanced tritium breeders by the emulsion method. Fusion Eng Des. 2014;89:1431–5. https://doi.org/10.1016/j.fusengdes.2013.12.052
35. Guo H, Wang H, Chen R, Gong Y, Yang M, Ye D, et al. Characterization of Li-rich Li_2TiO_3 ceramic pebbles prepared by rolling method sintered in air and vacuum. J Nucl Mater. 2021;546:152786. https://doi.org/10.1016/j.jnucmat.2021.152786
36. Guo H, Shi Y, Lu Z, Wang G, Deng M, Wang H, et al. Fabrication of submicron Li-rich $Li_2(Ti,Zr)O_3$ solid solution ceramics with sluggish grain growth rate. J Am Ceram Soc. 2022;106:738–51. https://doi.org/10.1111/jace.18781
37. Kimura T, Dong Q, Yin S, Hashimoto T, Sasaki A, Sato T. Synthesis and piezoelectric properties of Li-doped $BaTiO_3$ by a solvothermal approach. J Eur Ceram Soc. 2013;33:1009–15. https://doi.org/10.1016/j.jeurceramsoc.2012.11.007
38. Mukai K, Sasaki K, Hashimoto T, Suzuki A, Hoshino T, Terai T. Effect of Li/Ti ratio on microstructure and thermal diffusivity of lithium titanate for solid breeding material. Fusion Eng Des. 2011;86:2643–6. https://doi.org/10.1016/j.fusengdes.2011.01.054
39. Guo H, Shi Y, Wang H, Chen R, Ye D, Shi Q, et al. Characterization of cation disorder and oxygen vacancies in Li-rich Li_2TiO_3. J Am Ceram Soc. 2022;3:1–10. https://doi.org/10.1111/jace.18541
40. Kleykamp H. Enthalpy, heat capacity and enthalpy of transformation of Li_2TiO_3. J Nucl Mater. 2001;295:244–8. https://doi.org/10.1016/S0022-3115(01)00550-5
41. Christensen AU, Conway KC, Kelley KK. High-temperature heat contents and entropies of aluminates and ferrites of lithium and sodium, and of lithium titanate (US Bureau of Mines Rept Invest No 5565); 1960. p. 1–7.
42. He Y. Heat capacity, thermal conductivity, and thermal expansion of barium titanate-based ceramics. Thermochim Acta. 2004;419:135–41. https://doi.org/10.1016/j.tca.2004.02.008
43. Sohrabi Baba Heidary D, Lanagan M, Randall CA. Contrasting energy efficiency in various ceramic sintering processes. J Eur Ceram Soc. 2018;38:1018–29. https://doi.org/10.1016/j.jeurceramsoc.2017.10.015
44. Ibn-Mohammed T, Randall CA, Mustapha KB, Guo J, Walker J, Berbano S, et al. Decarbonising ceramic manufacturing: a techno-economic analysis of energy efficient sintering technologies in the functional materials sector. J Eur Ceram Soc. 2019;39:5213–35. https://doi.org/10.1016/j.jeurceramsoc.2019.08.011

SUPPORTING INFORMATION

Additional supporting information can be found online in the Supporting Information section at the end of this article.

How to cite this article: Mukai K. One-step fabrication of Li_2TiO_3 ceramic pebbles using pulsed YAG laser. J Am Ceram Soc. 2023;1–8. https://doi.org/10.1111/jace.19289